Physica B 172 (1991) 329–338
North-Holland

Diffraction of very cold neutrons at phase gratings

Kurt Eder, Manfred Gruber and Anton Zeilinger
Atominstitut der Österreichischen Universitäten, Schüttelstraße 115, A-1020 Wien, Austria

Roland Gähler
Physik-Department E21, Technische Universität München, D-8046 Garching, Germany

Walter Mampe
Institut Laue–Langevin, B.P. 156X, F-38042 Grenoble, France

Received 1 December 1990

We report extensive experiments on the diffraction of very cold neutrons ($\lambda \approx 100$ Å) at large-area transmission phase gratings with grating constants $d = 2$ μm and $d = 1$ μm, respectively. The experimental results are compared with Fresnel–Kirchhoff calculations showing agreement in great detail. Using phase gratings it is possible to shift intensities between different diffraction orders, thus making them very useful for other neutron-optics experiments at low energies. Also, the excellent manufacturing precision of our transmission phase gratings meets the requirements for such experiments like very-cold-neutron interferometry.

1. Introduction

For the development of a Mach–Zehnder-type interferometer for $\lambda = 100$ Å neutrons [1] new neutron-optics devices had to be tested at the new very-cold-neutron (VCN) optics facility at ILL [2]. We chose transmission phase gratings as beam splitting devices. Thus, extensive experiments had to be performed in great detail to find gratings of satisfactory quality for our neutron interferometer.

Recently, Baumann et al. published results on the diffraction of $\lambda = 20$ Å neutrons by transmission absorption gratings [3]. Diffraction by reflection gratings has been observed for thermal neutrons [4] and ultra-cold neutrons [5]. Various investigations of neutron diffraction using macroscopic objects other than gratings have also been reported [6].

2. Experimental set-up

The experiments were performed on the optical bench of the new VCN optics facility [2] at the Institut Laue–Langevin, Grenoble. This bench is mounted at the exit of the VCN port which uses half the cross-section of the neutron beam emerging from the TGV neutron guide that is connected to the new vertical cold-neutron source of the Grenoble high-flux reactor. The other half feeds a neutron turbine which produces ultra-cold neutrons. The optical table is of a honeycomb structure and is supported by pneumatic vibration isolation legs. Both are necessary to avoid the effect of background vibration on the operation of any optical device mounted on top of the bench. Its structure also reduces influences from internal temperature gradients. The table has a size of 6×1.2 m.

The set-up for our experiment is seen in fig. 1. The neutrons leave the VCN port having a broad wavelength distribution with a peak wavelength of about 60 Å. There, the beam has a cross-section of $17 \times 70\,\mathrm{mm}^2$. The VCN are then reflected by a 2000 Å thick nickel mirror which is set at a grazing angle of approximately 10°. This is also the critical angle for external total reflection of $\lambda \approx 100$ Å neutrons. Thus, short wavelength neutrons preferably just pass through the mirror and, therefore, are cut off from the original wavelength distribution. Hence we obtain spectra with a peak wavelength around 100 Å. Figure 2 shows a typical neutron spectrum measured with a time-of-flight technique. The sharp narrow maxima and minima at short wavelengths arise from constructive and destructive interference of waves reflected at the front face and the back face of the nickel mirror.

Slits S_1 and S_2, both having a width of 1 mm, define the width, the angular divergence and the wavelength distribution of the neutron beam (since the latter depends on the direction of the beam). Thus, the wave front incident to the phase grating situated just behind slit S_2 has an area of $1 \times 70\,\mathrm{mm}^2$. The 1 mm wide scanning slit S_3 and the neutron detector are mounted on a translation stage 1.632 m downstream from the grating. Between S_1 and S_2 and between the diffraction grating and S_3 we placed helium-filled tubes in order to avoid neutron losses due to scattering and absorption in air. The aluminum windows of the tubes had to be kept very thin (9 μm) to minimize small angle scattering effects in the windows. Also, the neutron counter, a

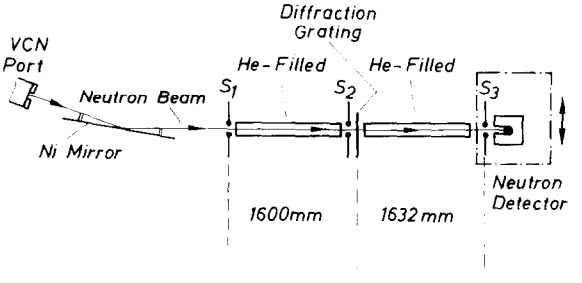

Fig. 1. Sketch of the experimental set-up (not drawn to scale). The neutron detector and slit S_3 are scanned along the scattering vector during the measurement.

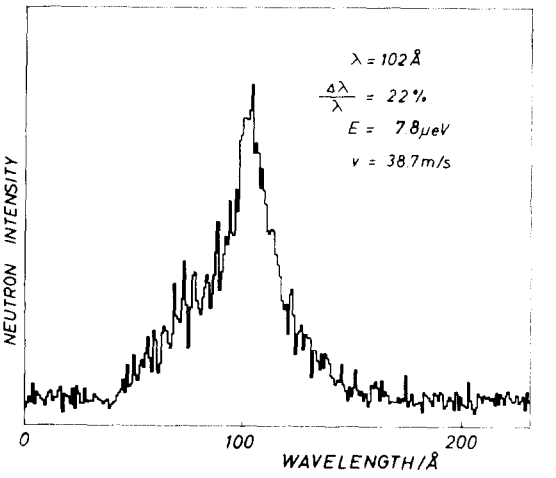

Fig. 2. Typical spectrum of VCN emerging from the TGV neutron guide at ILL after reflection at the 2000 Å nickel mirror (grazing angle nominally 10°) obtained by a time-of-flight technique.

BF_3 detector, has been shielded against background radiation. All slit edges are made of cadmium; the slits and the grating were each mounted on combinations of precision rotation and translation tables permitting the alignment of these optical elements. The alignment was achieved by means of a theodolite and a laser ruler

The translation stage with both the scanning slit S_3 and the detector was shifted along the diffraction vector by a step-motor-driven micrometer screw. The position of the stage was controlled by an optical encoder. At each position the neutron intensity was counted during measurement times of typically 500 s. The whole measurement procedure was supervised and controlled by a personal computer.

3. Theoretical considerations

Diffraction effects are best explained on the basis of the wave nature of the neutrons. According to Huygens' principle, every point of a wave front may be considered as a centre of a secondary disturbance which gives rise to spherical wavelets, and the wave front at any later instant may be regarded as the envelope of these

wavelets. This is a simple intuitive picture which permits an "understanding" or interpretation of the Fresnel–Kirchhoff diffraction formula which may be derived directly from the scalar wave equation

$$(\nabla^2 + k^2)U = 0 \tag{1}$$

by application of Green's theorem. This derivation is a standard one, reproduced in many physics texts and will not be repeated here (e.g. [7]).

Due to the vertical symmetry of our experiment we could restrict the computation of the Fresnel–Kirchhoff diffraction formula to two dimensions, i.e. neglect the vertical direction. Therefore, we also could neglect the influence of gravity on the very cold neutrons, although they fall about 5 cm in the earth's gravitational field on the path from the VCN port to the detector. The amplitude at a given point η in the plane of observation due to a point source at position σ in the entrance slit S_1 is

$$U(\eta, \lambda, \sigma) \sim \int e^{ik(r+s)} f(\xi)\, d\xi\,, \tag{2}$$

where r is the length of the path from the source point to a point ξ in the diffraction plane (object) and s the length of the path from there to the point of observation η. The integration is done over the width of the aperture enclosing the diffracting object. The transmission function $f(\xi)$ describes the influence of the object, i.e. the modification of the plane wave $\lambda = 2\pi/k$ incident to the diffracting object. This function is in general complex, since both the amplitude and the phase of the wave may be altered on passing through the object. If it alters the phase but not the amplitude (i.e. $|f(\xi)| = 1$) we speak of a phase object. Then $f(\xi) = \exp(i\phi(\xi))$ with $\phi(\xi)$ denoting the phase shift. For an amplitude object only the amplitude is altered (then $\arg(f(\xi)) = 0$).

Equation (2) describes a coherent summing over the individual paths through the diffracting object. Initially we consider the entrance slit S_1 to be illuminated with a single plane wave, which implies a coherent sum over the individual source points σ in the entrance slit. Therefore the amplitude at the point of observation η (due to a single plane wave incident on S_1) becomes

$$U(\eta, \epsilon, \lambda) \sim \iint e^{ik(r+s)} f(\xi) g(\epsilon)\, d\xi\, d\sigma\,, \tag{3}$$

with $g(\epsilon)$ describing the variation of the relative phase of the source points excited by the plane wave incident at angle ϵ.

The integration over the distribution $v(\epsilon)$ of the different incident directions of the wave front present, i.e. over the angular divergence of the radiation, was then performed on the intensity level. For $v(\epsilon)$ we assumed a Gaussian distribution with a FWHM defined by the geometry of slits S_1 and S_2. This means that neutrons incident from different directions onto the entrance slit S_1 were assumed to be incoherent with respect to each other. Likewise, the integration over the wavelength distribution $w(\lambda)$ (e.g. fig. 2) was also done incoherently. This assumption is justified because a static experiment can never reveal the wave-packet nature of the radiation studied [8, 9]. In a final integration step the finite width of the exit slit S_3 had to be taken into account by summation over exit slit points η, which simply is a convolution integration. The final intensity for a given position of the exit slit therefore is

$$I \sim \iiint |U(\eta, \epsilon, \lambda)|^2 v(\epsilon) w(\lambda)\, d\lambda\, d\epsilon\, d\eta\,. \tag{4}$$

In order to reduce the computation time on our computer we used the Fresnel approximation of eq. (2); i.e. the exact integral is substituted by Fresnel integrals, which can be evaluated through power series [7]. The theoretical intensity distributions thus obtained were then used in the comparison with the experimentally determined diffraction patterns.

The much simpler Fraunhofer approximation would only hold, if

$$D \ll s\,\frac{\lambda}{D}\,, \tag{5}$$

otherwise, the width D of the diffracting object

would be much greater than the width $s(\lambda/D)$ of the diffracted beam at distance s in the plane of observation. Although, for the numbers of our experiment ($D = 1$ mm and $s(\lambda/D) \approx 0.016$ mm), condition (5) is not satisfied, the Fraunhofer approximation is good enough to study the basic features of our gratings. Consider a diffracting object of infinite width that has an arbitrary periodic transmission function $f(\xi)$ with a period d. Also, permit only one wavelength λ_0 for the incoming wave, neglect any angular divergence ϵ and set the width of the entrance and the exit slit to ∞, i.e. no convolution with both slits is applied. Then, according to the Fraunhofer approximation, eq. (4) reduces to

$$I(\kappa) = I_0 H(\kappa) |F(\kappa)|^2 , \tag{6}$$

where I_0 denotes the incident intensity, $\kappa = d/\lambda_0 \cdot \sin(\vartheta)$ the normalized diffraction angle (ϑ is the true diffraction angle) and $H(\kappa)$ the interference function. $F(\kappa)$ is the Fourier transform of the transmission function $f(\xi)$ in one period d. $|F(\kappa)|^2$ is called the grating form factor; it modulates the interference function $H(\kappa)$. The latter exhibits the periodicity of the transmission function. $H(\kappa)$ has its maxima at angles $\kappa = n$ where n is an integer; for an object of infinite width it simply is $\Sigma_n \delta(\kappa - n)$, a sum of Dirac's delta functions.

For our new VCN interferometer [1] it was decided to use a Mach–Zehnder topology with transmission phase gratings, which clearly are preferred to absorption gratings for intensity reasons. If one employs such an interferometer with gratings, it is advantageous to use zero-order and first-order diffraction only. Therefore it would be preferable to avoid losing too much intensity into higher orders. Since, in simple cases, higher-order intensities decrease by the square of the number of order anyway, specifically the second-order intensity should be kept as low as possible. As stated above, the transmission function for a pure phase object has the form $f(\xi) = \exp(i\phi(\xi))$. In our case, a grating profile with steps and grooves of equal width and rectangular shape was chosen, then $\phi(\xi)$ is a square-wave function with period d. The phase shift is determined by the height h of the steps and the λ-thickness D_λ, i.e. that thickness of a

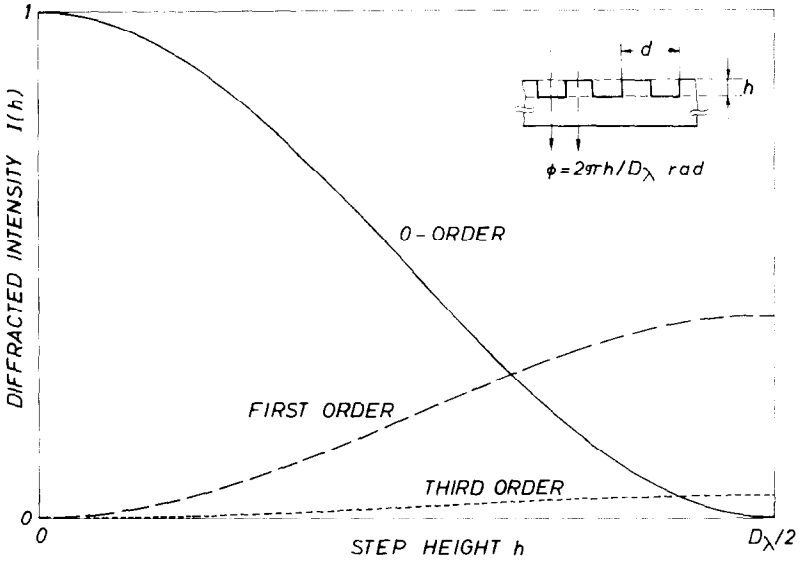

Fig. 3. Intensities for three of the first four orders of the diffraction at a phase grating (grating constant d) with equal width of steps and grooves as a function of the step height h. The second order is zero for all possible phase shifts (solid: zero order, dashed: first order, and short-dashed: third order).

particular material which leads to a phase shift of 2π rad,

$$\phi = 2\pi \frac{h}{D_\lambda} . \tag{7}$$

Figure 3 shows the dependence of the grating form factor $|F(\kappa)|^2$ on the step height h for the first four diffraction orders, for this particular grating geometry. The chosen profile achieves the goal of reducing the second-order intensities perfectly well; in fact, all even-order diffracted maxima are suppressed. Also, fig. 3 exhibits an important feature of phase gratings, since for them the distribution of intensity between different orders can be manipulated, while for absorp-

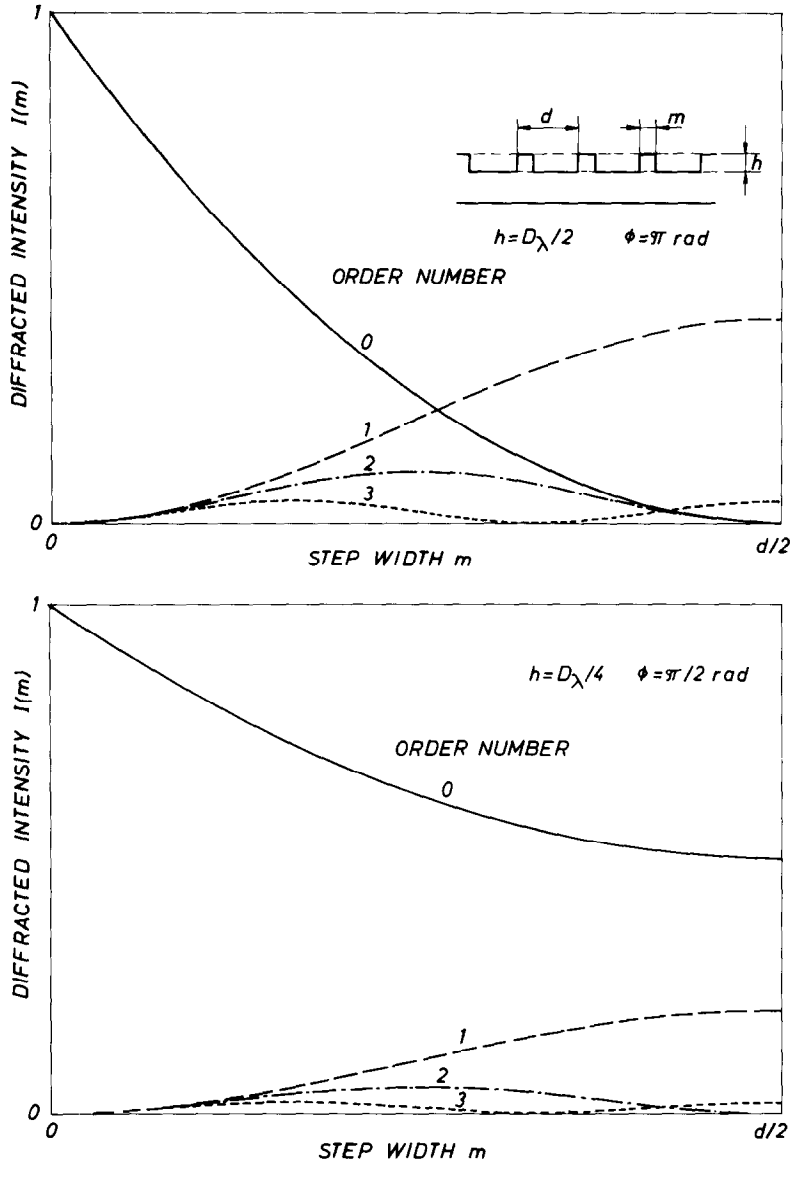

Fig. 4. Intensities for the first four orders of the diffraction at a phase grating (grating constant d) with rectangular steps of varying width m and a height h of the steps corresponding to phase shifts $\phi = \pi$ rad (a) and $\phi = \pi/2$ rad (b) (solid: zero order, dashed: first order, dash-dotted: second order, and short-dashed: third order).

tion gratings this intensity ratio is fixed. The zero-order maximum is a superposition of transmitted waves with relative phase ϕ. Clearly, if the amplitudes of the two waves are equal, which is the case for a grating with a step-to-groove width ratio of 1:1, and if $\phi = \pi$ rad (i.e. $h = D_\lambda/2$), the zero-order maximum is canceled. This is the choice for the second grating of our interferometer, since there only first-order diffraction is needed and the zero-order diffraction

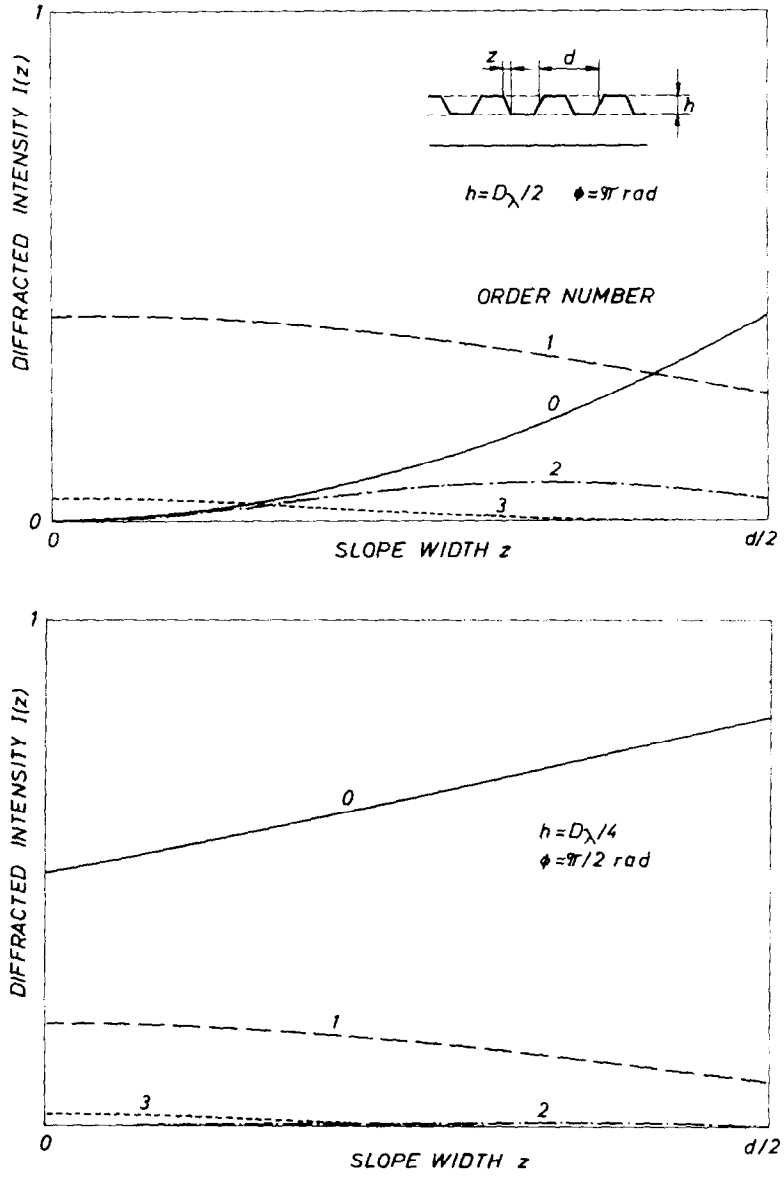

Fig. 5. Intensities for the first four orders of the diffraction at a phase grating (grating constant d) with steps of trapezoid with varying width z of the slopes and a height h of the steps corresponding to phase shifts $\phi = \pi$ rad (a) and $\phi = \pi/2$ rad (b width m of the steps is equal to $d/2$ (solid: zero order, dashed: first order, dash-dotted: second order, and short-dashed order).

intensities would not contribute to the interference pattern. The first and the third grating employ both a zero-order and a first-order diffraction. For intensity reasons two $\pi/2$-gratings were selected for these two gratings, where $\pi/2$ refers to the selected phase shift; then the transmitted intensity is maximal. But as the λ-thickness D_λ depends on the wavelength, these phase shifts can be met for one particular λ only.

Due to limitations of the manufacturing process exact rectangular steps could not be achieved. Then, a good approximation of the square-wave transmission function $f(\xi)$ is a trapezoid-wave function where the steps are of trapezoid shape with a height h, a width at half-height m (which is not necessarily equal to $d/2$) and two slopes of width z. Figure 4 shows the influence on the grating form factor for the first four diffraction orders of a π- and a $\pi/2$-grating due to variations of the step width m, neglecting possible slopes of width z ($z = 0$). The ideal case is given by $m = d/2$. Clearly, for $m = 0$ no diffraction occurs, since then the steps have vanished. A step-to-groove ratio of 1:3 is represented in the center of the plots by $m = d/4$. The influence of trapezoidal deviations z of steps of constant width $m = d/2$ are seen in fig. 5. Here, $z = 0$ marks the ideal case, and for $z = d/2$ the trapezoid has deformed to a triangle with equal legs. Deviations from the ideal case – wider or narrower steps and/or trapezoidal distortions – always contribute to a higher zero-order maximum, lower the first-order intensities and generate non-zero even orders. The former can be remedied by an improved manufacturing process. In the case of $\pi/2$-gratings we decided for higher steps, i.e. a phase shift of more than $\pi/2$ rad, since then the effects mentioned above are corrected to some extent, because bigger phase shift means lower zero-order and higher first-order maxima. For π-gratings there is no such remedy. But, even with an ideal profile, if one has to cope with a broad wavelength distribution, one has to accept a non-ideal distribution of the diffracted intensities. As stated above, the phase shift ϕ depends both on height h and neutron wavelength λ, so a particular ϕ can only be achieved for one particular λ and h.

4. The gratings*

In order to achieve appreciable diffraction angles for $\lambda = 100$ Å neutrons one has to use structures of micrometer size. Thus, we chose grating constants $d = 1\,\mu$m and $d = 2\,\mu$m, respectively. The low neutron flux necessitates a large area ($13 \times 80\,\text{mm}^2$) for the gratings. As optical reduction of a mask of different size would produce unavoidable aberrations one has to use a mask with the same size and grating period as the final gratings. This implies the need for high precision of the mask manufacturing process. The gratings were supported by SiO_2 glass plates of thickness $t = 2.5$ mm. The thickness has to be constant over the whole area of the plate to avoid different phase shifts for neutrons passing through different parts of the plates. The λ-thickness of quartz glass, which corresponds to a phase shift of 2π rad, is $D_{100\text{Å}} = 1.7\,\mu$m; thus, we used plates where the thickness was constant to better than $\pm 0.025\,\mu$m ($\lambda_{\text{light}}/10$).

For a first series of 2 μm gratings a diamond tip which is controlled by a light interferometer ruled a gold foil to produce a master mask. By this means the error of the grating period d could be kept as a low as 100 Å over the whole area of the grating. By an electroplating process nickel steps were brought onto the quartz-glass plates. But, due to the abrasion of the diamond tip (the tip has to travel 500 m to rule the whole mask!), the step-to-groove width ratio of the mask changed from 1:1 to 3:1, which, of course, is not satisfactory.

For a second series of gratings a new mask was made by use of electron lithography. This time, copper was electroplated onto the SiO_2 glass substrate, because of possible variations of the magnetization of the nickel steps. Unfortunately, due to the large area of the mask it was impossible to produce it as one piece; it had to be joined together from smaller parts. This resulted in stacking faults at the joints of those parts. Furthermore, oxidation of the copper structures and other unknown imperfections due to the

* The gratings were manufactured by Dr. J. Heidenhain GmbH, D-8225 Traunreut, Germany.

complicated manufacturing process caused severe problems. All those facts made the gratings unsatisfactory for interferometer use.

Finally, for a third series, mask 1 from the first series was chosen again, but this time the photo resist was exposed twice. After the first exposure the mask was rotated by 180° and then it was exposed a second time, thus averaging possible variations of step width m. Grooves were then sputter-etched into the SiO_2 glass. By this process good quality gratings could be obtained. The 1 μm gratings were produced the same way but by using, of course, a different mask.

5. Experimental results

A wavelength $\lambda \approx 100$ Å and a grating constant $d = 2$ μm lead to a first-order scattering angle $\vartheta \approx 5 \times 10^{-3}$ rad. This results for our set-up (s = 1632 mm) in a splitting of the neutron beam of about 8 mm. The beam divergence chosen by the geometry of the slits S_1 and S_2 leads to a broadening of the beam profiles. Furthermore, one expects an additional broadening of the non-zero diffraction orders due to the broad wavelength distribution ($\Delta\lambda/\lambda = 22\%$) we had to use, since the scattering angle ϑ depends also on the wavelength. The latter effect and the wavelength dependence of the phase shift of the grating also distort the profiles of the non-zero maxima: long-wavelength neutrons are diffracted to the "far side" (bigger scattering angle) of the peaks. The intensity distribution between different orders due to the phase shift in the phase grating (fig. 3) differs in general from the one of the short-wavelength neutrons on the "near side" – even if the original wavelength distribution of the neutrons would be symmetrical. Of course, our nonsymmetrical distribution of neutron energies (fig. 2) contributes to a distortion of the peaks, too. All above effects are well observed in all patterns. Thus, if one wants to compare different order intensities, one has to compare the peak areas. Also, in our calculations we neglected trapezoidal imperfections, i.e. $z = 0$.

For the experiments with the series I and II gratings we chose a peak wavelength of 107 Å. Figure 6 shows a typical measurement of a series I grating. The nickel steps had a height of 0.38 μm which corresponds to a phase shift of 1.22 π rad ($D^{Ni}_{107Å} = 0.623$ μm). For the numerical calculation a step width $m = 1.40$ μm had to be assumed to fit the data. These imperfections and the wavelength distribution (see above) contribute to a large first-order maximum. But as stated in section 4, the deviation of the step width m strongly varied with the illuminated area of the grating.

The diffraction pattern of a series II grating (fig. 7, 0.48 μm Cu, $D^{Cu}_{107Å} = 0.900$ μm) shows that, although the step-to-groove width was nearly 1:1 as could be seen by means of a microscope, other grating faults as oxidation and stacking faults (see section 4) contributed to a large "numerical" deviation $m = 1.25$ μm from the ideal case $m = 1$ μm.

We chose a slightly different peak wavelength of 102 Å for the measurements with our SiO_2 glass gratings; then $D^{quartz\text{-}glass}_{102Å} = 1.768$ μm. The diffraction pattern of a grating with a step height of 0.58 μm exhibits a satisfactory result (fig. 8). Similar results were also met by other gratings of different phase shifts. There is also only a very small second-order maximum stemming from im-

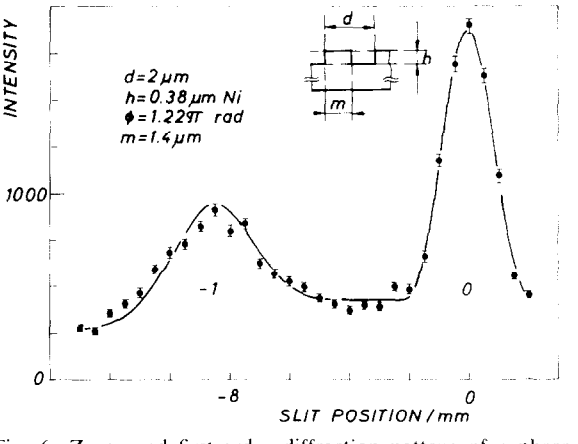

Fig. 6. Zero- and first-order diffraction pattern of a phase grating with nickel steps ($D^{Ni}_{107Å} = 0.623$ μm) and a grating constant $d = 2$ μm. The solid line represents a numerical calculation (refer to text).

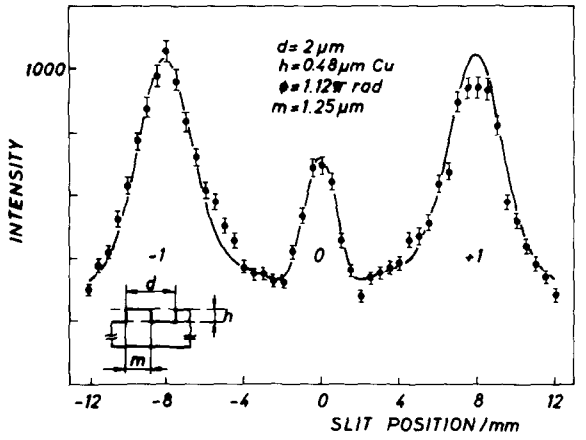

Fig. 7. Zero- and first-order diffraction pattern of a phase grating with copper steps ($D^{Cu}_{107Å} = 0.900\,\mu m$) and a grating constant $d = 2\,\mu m$. The solid line represents a numerical calculation (refer to text).

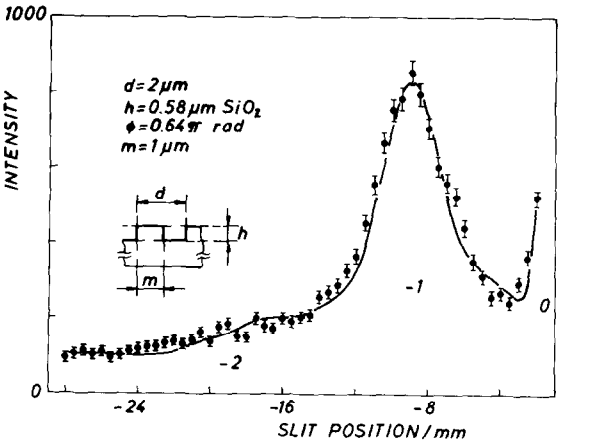

Fig. 9. First- and second-order diffraction pattern of a phase grating with quartz-glass steps ($D^{quartz\text{-}glass}_{102Å} = 1.768\,\mu m$) and a grating constant $d = 2\,\mu m$. The solid line represents the numerical calculation (refer to text).

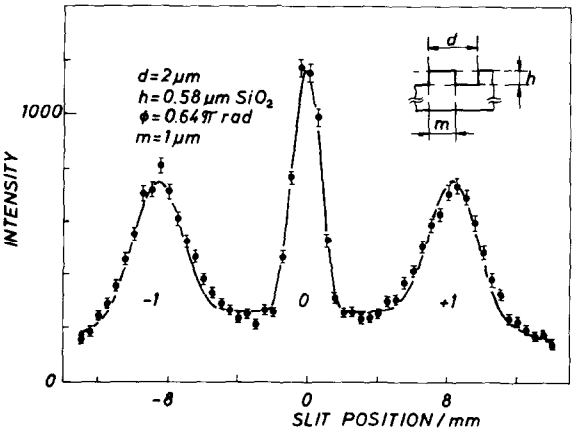

Fig. 8. Zero- and first-order diffraction pattern of a phase grating with quartz-glass steps ($D^{quartz\text{-}glass}_{102Å} = 1.768\,\mu m$) and a grating constant $d = 2\,\mu m$. The solid line represents the numerical calculation (refer to text).

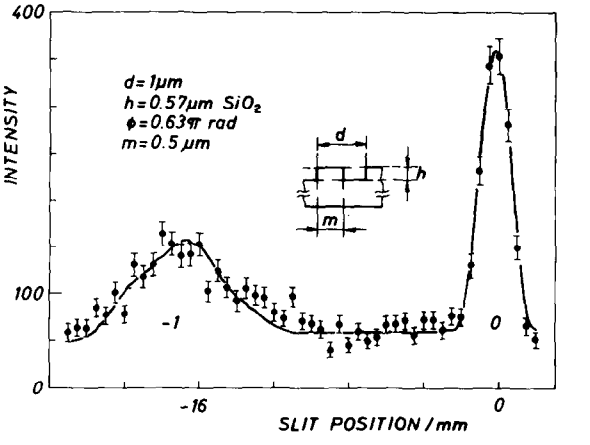

Fig. 10. Zero- and first-order diffraction pattern of a phase grating with quartz-glass steps ($D^{quartz\text{-}glass}_{102Å} = 1.768\,\mu m$) and a grating constant $d = 1\,\mu m$. The solid line represents the numerical calculation (refer to text).

perfections (fig. 9) which shows the good manufacturing quality of the gratings. Figure 10 displays the diffraction of a grating with a period $d = 1\,\mu m$ and a step height $h = 0.57\,\mu m$. In this case the first-order peak widens dramatically due to the greater diffraction angle. The waviness of the line of the numerical calculations stems from the behavior of the Fresnel approximation.

6. Conclusion

We have shown that it is possible to obtain large-area diffraction gratings to the precision required for the work with very cold neutrons. In particular, we think that all features of the diffraction patterns are well understood and that it therefore is possible to use phase gratings to shift

the intensities between different diffraction orders as needed by the specific requirements of the experiment. We would also like to point out that standard Fresnel–Kirchhoff calculation leads to a satisfying quantitative agreement with experimental observation. It is not unreasonable to expect that such diffraction gratings will play a major role in future neutron-optics experimentation at very low energies.

Acknowledgements

We would like to thank the Institut Laue–Langevin for giving us the possibility of performing these experiments, and in particular Dr. W. Drexel for continuing support. We thank Professor C.G. Shull (M.I.T.) for stimulation and encouragement and Professor H.J. Bernstein (Amherst) for discussions. We also appreciate the constructive cooperation of Herr Heinz Kraus from Heidenhain Company in the development of the phase gratings. This work was mainly supported by the Austrian Fonds zur Förderung der wissenschaftlichen Forschung under project No. P 6635 T. Additional support was received from the Bundesministerium für Forschung und Technologie (Bonn) and from the US National Science Foundation (grants No. DMR 87-13559 and No. INT-87-13341).

References

[1] M. Gruber, K. Eder, A. Zeilinger, R. Gähler and W. Mampe, Phys. Lett. A 140 (1989) 363.
[2] K. Eder, M. Gruber, A. Zeilinger, R. Gähler, W. Mampe and W. Drexel, Nucl. Instr. and Meth. A 284 (1989) 171.
[3] J. Baumann, J. Kalus and W. Mampe, Nucl. Instr. and Meth. A 284 (1989) 184.
[4] H. Kurz and H. Rauch, Z. Physik 220 (1969) 419.
[5] H. Scheckenhofer and A. Steyerl, Phys. Rev. Lett. 39 (1977) 1310.
[6] For a complete reference, see A.G. Klein and S.A. Werner, Rep. Prog. Phys. 46 (1983) 259.
[7] M. Born and E. Wolf, Principles of Optics, 6th ed. (Pergamon, New York, 1980).
[8] A.G. Klein, G.I. Opat and W.A. Hamilton, Phys. Rev. Lett. 50 (1983) 563.
[9] H.J. Bernstein and F.E. Low, Phys. Rev. Lett. 59 (1987) 951.